Anti-Jamming Front-End Design of Satellite Navigation Receiver

Fan Wang, Haipeng Liu, and Chuanfang Zhang

School of Information and Electronics
Beijing Institute of Technology, Beijing, 100081, China
zcf@bit.edu.cn, wangfan@bit.edu.cn

Abstract ─ In this paper, an anti-jamming front-end is proposed for the satellite navigation receiver. Firstly, a seven-element receiving antenna array and an eight-channel (seven receiving channels and one calibration channel) radio frequency (RF) module are devised. Then, the interference suppression module based on the linear constraint minimum variance (LCMV) criterion are designed and analyzed. By using the LCMV-PI algorithm, the spatial domain information of the signal can be used to effectively suppress the interference. In addition, considering that the channel inconsistency will adversely affect the interference suppression algorithm and subsequent signal acquisition and tracking, a channel equalization scheme is devised to correct the channel inconsistency.

Index Terms ─ Antenna array, anti-jamming, channel equalization, LCMV-PI algorithm, RF module.

I. INTRODUCTION

During the last several decades, the satellite navigation system has been widely used in aerospace, navigation, transportation, meteorology, measurement and other areas. It plays a more and more important role in social and economic development with huge value. However, after the satellite signal reaches the ground, the power is as low as only about -130dBm which submerges under the noise of the satellite navigation receiver. In addition, with the electromagnetic propagation environment becoming more complex, the weak navigation signal is more susceptible to intentional or unintentional interference, which causes the failure for the receiver to locate accurately. Therefore, as an important indicator to measure the performance, the interference suppression capability of the satellite navigation receiver must be strong. Nowadays, the interference suppression technology has become one of the research focuses in the satellite navigation field.

There are two interference suppression techniques for satellite navigation receiver. One is based on single antenna and the other is based on antenna array [1-3]. Li and Milstein [4] applied a linear transversal filter to the spread-spectrum system and suppressed the narrow-band interference. Milstein [5] then proposed a method based on fast Fourier transform to suppress interference in the frequency domain. Rao and Kung [6] proposed an adaptive constrained infinite impulse response (IIR) filter for the enhancement and tracking of sinusoids in additive noise. Poor [7] made a summary of two code-aided method including linear code-aided method and maximum-likelihood code-aided method. Chang et al. [8] raised that the single antenna-based interference suppression method has a simple structure. But only narrow-band interference can be suppressed. For this reason, antenna array interference suppression technology is introduced, and the spatial domain characteristics of the signal are used to suppress the interference. Fante and Vaccaro [9] applied the spatial domain adaptive filtering algorithm based on the minimum power criterion to the satellite navigation receiver, which improved the ability of the receiver to suppress interference. Goldstein et al. [10] proposed a Multistage Wiener Filter method based on orthogonal projections. This method reduced the amount of computation caused by matrix inversion and improved the convergence speed of the interference suppression algorithm. In this paper, an anti-jamming front-end is designed in order to improve the interference suppression performance of satellite navigation receiver. Li et al. [11] developed a new reweighted l_1-norm and an l_p-norm based normalized least mean square algorithms for sparse adaptive array beamforming control applications. Choi et al. [12] described a new direct data domain least squares (D^3LS) method using real weights, which utilized only a single snapshot of the data for adaptive processing.

In this paper, the LCMV-PI interference suppression algorithm is firstly mathematically deduced. The Monte-Carlo simulation is used to analyze the effectiveness of the algorithm for two special cases. For the first case, the angle between the useful signal and interference signal is small; for the second case, the power of interference signal is extremely large. Then an anti-jamming receiving front-end is designed. The RF module is designed with a calibration channel to achieve the calibration of the amplitude and the phase consistency of the down-conversion channel. This design improves

Submitted On: June 27, 2019
Accepted On: September 10, 2019

the interference suppression performance in the actual use of the interference suppression algorithm. By comparing with the related literature, the performance of the LCMV-PI algorithm and the rationality of the front-end design are verified.

This paper is organized as follows. Section II introduces the LCMV-PI interference suppression algorithm and carries on simulations by Matlab. Section III briefly presents the architecture of anti-jamming front-end. And then the specific design of antenna array, RF module and interference suppression module are presented, respectively. The performance of the proposed anti-jamming front-end is tested in Section IV. Finally, section V gives the conclusion.

II. SPACE ADAPTIVE INTERFERENCE SUPPRESSION ALGORITHM DESIGN

A. Signal model of antenna array

An arbitrary antenna array structure of M array elements is shown in Fig. 1. The spatial three-dimensional coordinates of the mth array element are $\rho_m = [x_m, y_m, z_m]$. The incident angles of the signal are (θ, φ), where θ is the pitch angle and φ is the azimuth angle. R_0 is the distance between the source and the reference point. R_m is the distance between the source and the mth element. It can be seen that the distance from the mth array element to the reference point is $\vec{R_m} \triangleq R_m - R_0$. The propagation delay τ_m of the signal from the mth array element to the reference point is:

$$\tau_m = \frac{\vec{R_m}}{c} = \frac{1}{c}\left(x_m sin\theta cos\varphi + y_m sin\theta sin\varphi + z_m cos\theta\right) \quad m=0,1,\cdots,M-1. \tag{1}$$

The corresponding spatial phase difference is:

$$\phi_m(\theta,\varphi) = = \frac{2\pi}{\lambda}\left(x_m sin\theta cos\varphi + y_m sin\theta sin\varphi + z_m cos\theta\right) \quad m=0,1,\cdots,M-1. \tag{2}$$

Thus, the steering vector of the antenna array is:

$$a(\theta,\varphi) = \left[e^{-j\phi_0(\theta,\varphi)}\ e^{-j\phi_1(\theta,\varphi)}\ \cdots\ e^{-j\phi_{M-1}(\theta,\varphi)}\right]^T. \tag{3}$$

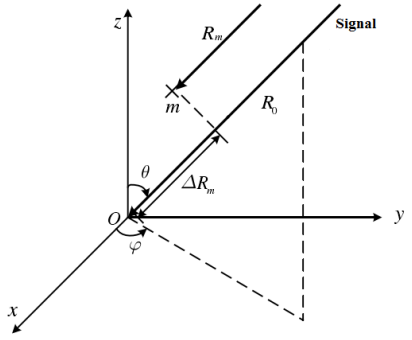

Fig. 1. Schematic diagram of arbitrary antenna array structure.

B. Analysis of LCMV-PI algorithm

The space adaptive anti-jamming processing consists of the antenna array and the adaptive processing algorithm. Figure 2 depicts the principle of the space adaptive anti-jamming processing. It can be seen that the basis of the adaptive processing is to adjust the weight vectors of the array elements according to the adaptive processing algorithm. By weighting and summing the signals received by each array element, the antenna array beam is "guided" to a certain direction where the useful signals are enhanced, and the interference signals are suppressed [13-17]. The output of the array is:

$$y(t) = \sum_{m=1}^{M} w_M{}^H x_m(t) = w^H x(t). \tag{4}$$

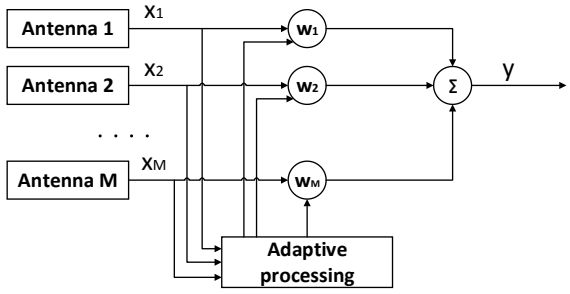

Fig. 2. The principle of the space adaptive anti-jamming processing.

The LCMV criterion is to minimize the output power of the array under some linear constraints. The cost function of the LCMV criterion is:

$$\min_w w^H R_{xx} w \quad s.t.\ w^H C = f, \tag{5}$$

where, C is the constraint matrix and f is the constraint response vector.

Based on the Lagrange multiplier method, the objective function is constructed as:

$$L(w) = w^H R_{xx} w - \lambda(f^H - C^H w), \tag{6}$$

where λ is the Lagrange multiplier.

Let $\nabla_w L(w) = 0$, the optimal weight vector is:

$$w_{opt} = R_{xx}{}^{-1} C (C^H R_{xx}{}^{-1} C)^{-1} f^H. \tag{7}$$

PI algorithm is based on the LCMV criterion. Let $C = [1,0,\cdots,0]^T = s_0$, $f = 1$, (5) can be rewritten as:

$$\min_w w^H R_{xx} w \quad s.t.\ w^H s_0 = 1. \tag{8}$$

Then, the optimal weight vector can be obtained as:

$$w_{opt} = \frac{1}{s_0{}^H R_{xx}{}^{-1} s_0} R_{xx}{}^{-1} s_0. \tag{9}$$

The PI algorithm ensures that the weight of the first channel is always 1, while the weights of the other channels are constantly modified during the iteration to meet the LCMV criterion. In the satellite navigation receiving system, the power of the interference signal is much larger than the useful signal, using the PI algorithm can form a deep zero-trap in the direction of interference

signal to achieve the suppression of interference and improve the SINR of the system.

C. Simulation of LCMV-PI algorithm

The performance evaluation of LCMV-PI interference suppression algorithm is conducted by simulation verification analysis based on Matlab. It is assumed that both the antenna array and the RF channel are ideal. The Monte-Carlo simulation is performed on the algorithm for three cases: the general case, the case in which the angle between the useful signal and the interference signal is very small, and the case in which the amplitude of the interference signal is extremely large.

For the general case, the simulation parameters are designed as:

(1) Antenna array setting: seven-element central circular array with the radius of 0.8λ;

(2) Useful signal direction: (10°, 10°);

(3) Interference signal direction: (80°, 80°);

(4) Interference signal setting: INR=80dB, ISR=100dB.

The radiation patterns of the antenna array are shown in Fig. 3. It can be seen that the radiation pattern forms a deep zero-trap in the direction of the interference signal, reaching -104dB. The effectiveness of the LCMV-PI algorithm for interference suppression is verified.

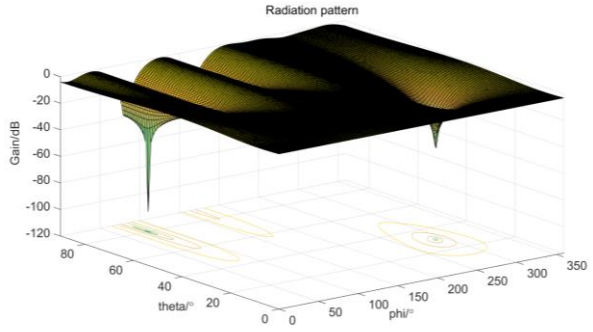

(a) Three-dimensional radiation pattern

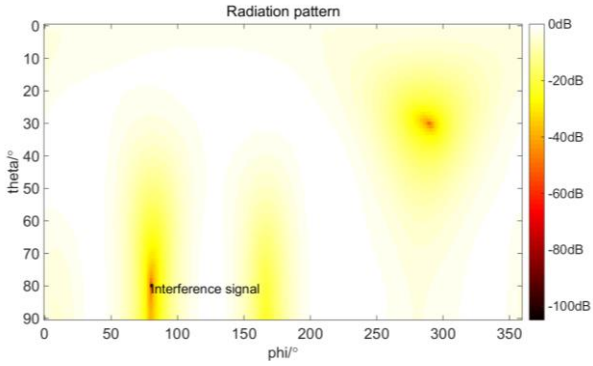

(b) Color map

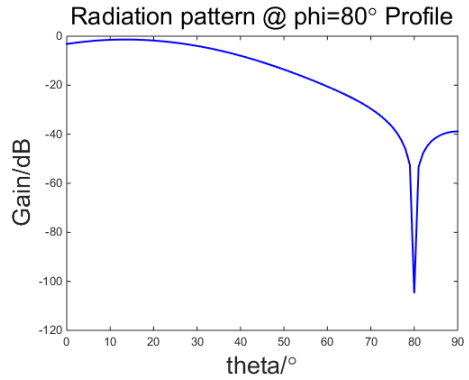

(c) Profile @phi=80°

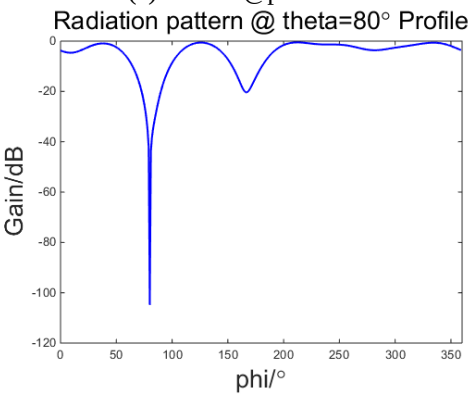

(d) Profile @theta=80°

Fig. 3. The radiation patterns of the antenna array by using LCMV-PI algorithm.

For the second case, the direction of the useful signal is set as (0°, 0°), and the angle between the useful signal and the interference signal is less than 5°. The remaining parameters remain unchanged. Figure 4 shows the radiation pattern in this case. It can be seen that a deep zero-trap is formed in the direction of the interference, reaching more than -95dB, which verifies the effectiveness of the algorithm.

For the third case, the ISR is set as 200dB, 250dB and 300dB, respectively. The remaining parameters remain unchanged. The Monte-Carlo simulation results are shown in Fig. 5. From the radiation pattern, it can be seen that the larger the amplitude of the interference signal is, the deeper the zero-trap formed by the algorithm will be. The effectiveness of the LCMV-PI algorithm is also verified. However, in practice, when the interference signal power is extremely large, the receiving channel is highly likely to be saturated. At this time, the AD cannot effectively sample the receiving signal, which in turn causes the failure of the interference suppression algorithm. To cope with this situation, multi-stage automatic gain control (AGC) can be added to the receiving channels to improve the dynamic range of the

receiving channels.

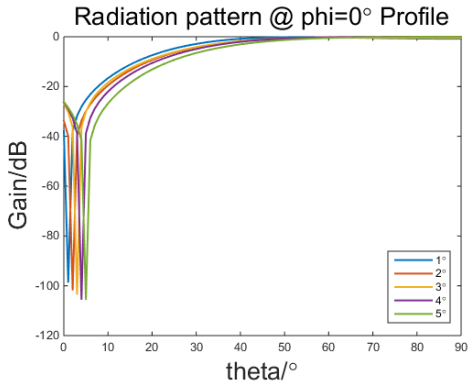

Fig. 4. The radiation pattern when the angle between the useful signal and the interference signal is small by using LCMV-PI algorithm.

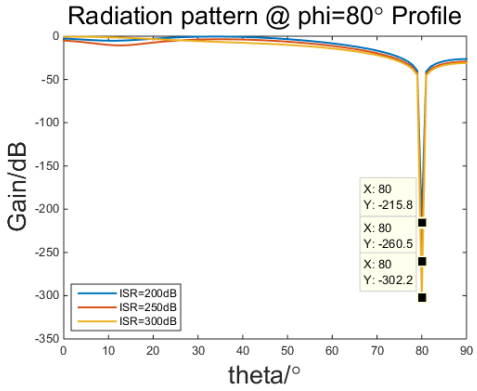

Fig. 5. The radiation pattern when the magnitudes of the interference signals are extremely large by using LCMV-PI algorithm.

III. ANTI-JAMMING FRONT-END DESIGN

The anti-jamming front-end is mainly composed of an antenna array, a RF module and an interference suppression module. The antenna array consists of seven antenna elements for receiving satellite navigation signals. The RF module consists of eight channels, seven of which are mainly used to down-convert the seven signals received by the antenna array to the IF and then send them to the interference suppression module for anti-jamming processing. The remaining channel up-converts the IF calibration signal of the baseband module to the L-band and adjusts the signal to an appropriate power level range. Thus, the signal can be used as a calibration signal for the seven receiving channels. The interference suppression module implements two functions of channel correction and interference suppression. It also transmits the anti-jamming processed IF signal to the back-end baseband module for acquisition and tracking. Figure 6 depicts the block diagram of the receiver system.

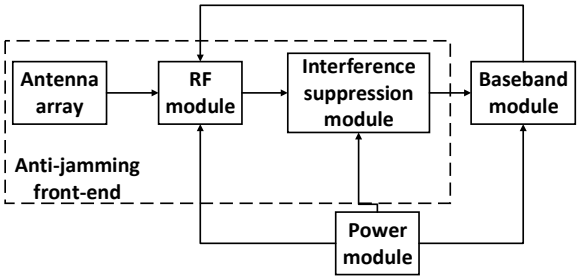

Fig .6. The block diagram of the receiver system.

A. Antenna array design

The antenna array is in the form of a seven-element central circular array, as shown in Fig. 7. The physical structure of the antenna array, that is, the relative position between the array elements, has a great influence on the performance of the entire system. When selecting the relative distance, the coupling effect between the antenna elements should be considered. When the spacing of the array elements is too small, a serious mutual coupling phenomenon will occur, which makes the interference suppression algorithm form a wider range and shallower depth of the zero-trap. And then the performance of interference suppression is reduced. When the spacing is too large, a large-scale scanning in the upper half of the antenna array may generate grating lobes, which is also undesirable for the system. On account of the considerations above and anti-jamming requirements, the mutual coupling should be minimized and the grating lobes appearing in the scanning space should be prevented in the simulation. Thus, the spacing is chosen as $\boldsymbol{R = 0.8\lambda}$, where $\boldsymbol{\lambda}$ is the free space wavelength.

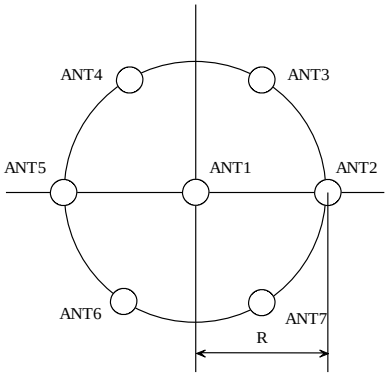

Fig. 7. Schematic diagram of the antenna array arrangement.

The consistency of the antenna elements has a certain impact on the performance of interference

suppression. Therefore, the seven antenna elements are designed in a unified form, and the un-roundness of the antenna elements and the isolation between the antenna elements are improved. The antenna element is in the form of the microstrip patch, as shown in Fig. 8.

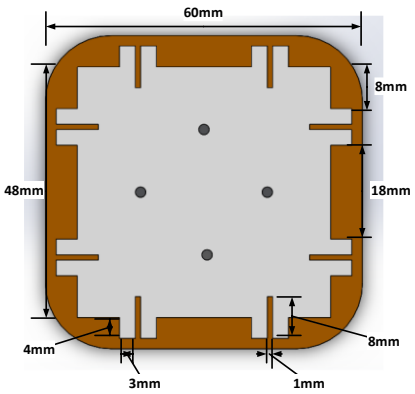

(a) The dimensions of the antenna element

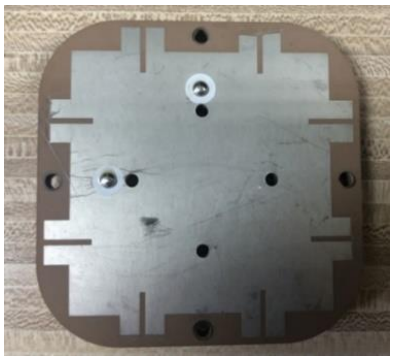

(b) The photo of the antenna element

Fig. 8. The prototype of the antenna element.

As shown in Fig. 9, ABS plastic (dielectric constant 3.3, loss tangent 0.001) is chosen to be the material of the radome. The thickness of the radome is 3mm. The overall height of the antenna array is 120mm and the diameter of the bottom aluminum substrate disk is 530mm.

(a) Top view

(b) Side view

Fig. 9. The prototype of the seven-element antenna array with radome.

When the center frequency is 1340.13MHz, the radiation pattern of the antenna element is shown in Fig. 10. The un-roundness of the antenna element on theta=60° is shown in Fig. 11. From these two graphs, it can be gained that the zenith gain of the antenna element reaches 7.68dB; the 3dB lobe width reaches 75°; the 6dB lobe width reaches 110°; the front-to-back ratio is -22.2dB; the un-roundness is better than 2dB on theta=60°.

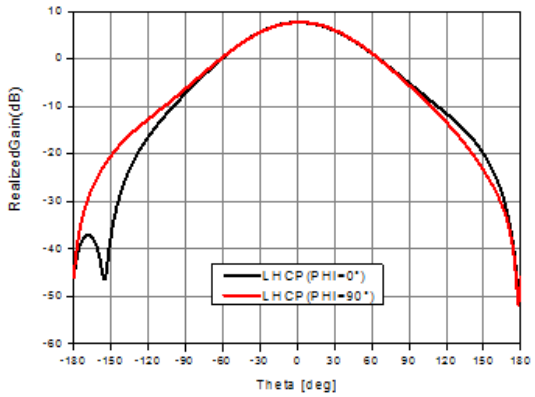

Fig. 10. The radiation pattern of the antenna element at 1340.13MHz.

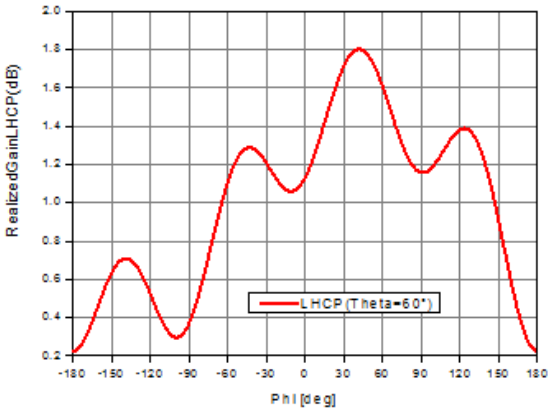

Fig. 11. The un-roundness of the antenna element on theta=60° at 1340.13MHz.

Figure 12, Fig. 13 and Fig. 14 depict the radiation pattern, the isolation and the axial-ratio of the antenna array, respectively. It can be obtained that the zenith gain of the antenna array reaches 16.39dB; the 3dB lobe width reaches 26°; the 6dB lobe width reaches 36°; the isolation is better than -26dB; the axial-ratio is better than 0.6dB.

B. RF module design

As shown in Fig. 15, the RF module is mainly composed of three sub-modules: receiving down-conversion module, transmitting up-conversion module and local oscillator module. Figure 16 shows the prototype of the RF module.

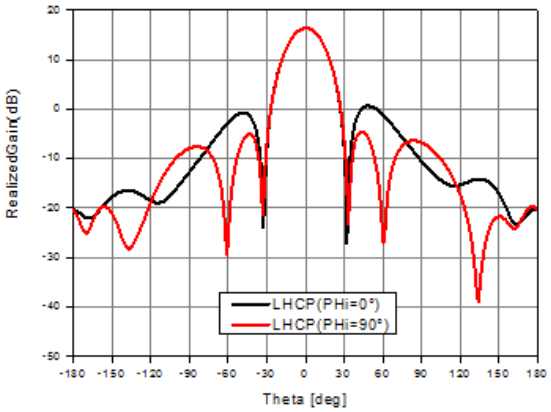

Fig. 12. The radiation pattern of the antenna array at 1340.13MHz.

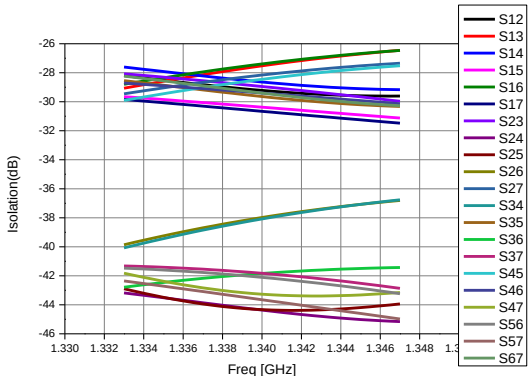

Fig. 13. The isolation between the antenna elements.

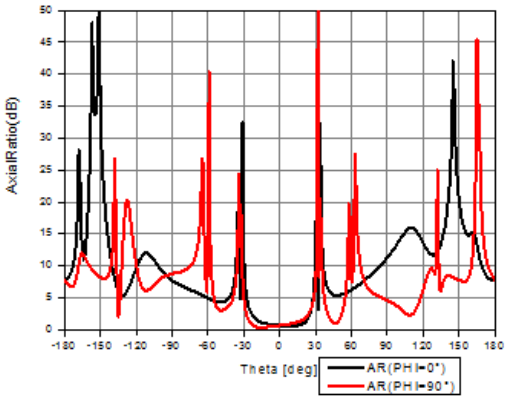

Fig. 14. The axial-ratio of the antenna array at 1340.13MHz.

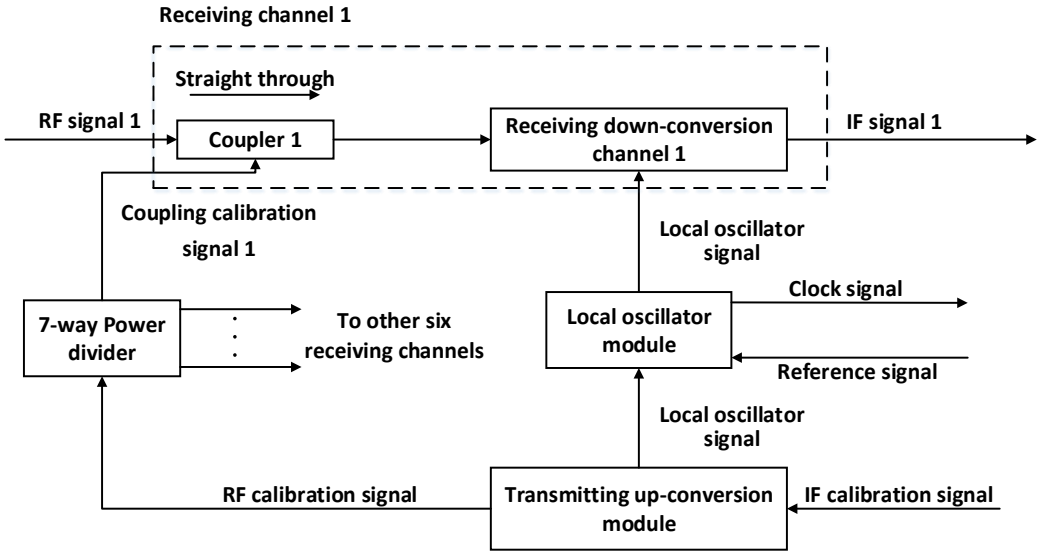

Fig. 15. The block diagram of the RF module.

Fig. 16. The prototype of the RF module.

The receiving down-conversion module consists of seven receiving channels with same frequency and gain configuration. The receiving channel adopts the classic super-heterodyne structure. The L-band RF signal of 1340.13MHz received by the seven-channel L-band receiving antenna array is converted to the 70.13MHz IF signal and then transmitted to the interference suppression module for anti-jamming processing.

The working principle of the receiving channel is shown in Fig. 17. After the RF signal entering the receiving channel, the first stage is an isolator (Hongda's HGD09S1.25-1.35G) that guarantees the standing wave indicator of the RF port. The second stage is a coupler (RN2's RCP1500A30) for coupling the calibration signal. The third stage is a low noise amplifier (LNA, Qorvo's TQP3M9036), which is cascaded by a two-stage amplifier to ensure the noise figure (NF) of the receiving channel. A two-stage band-pass filter (Jiangjia's MC4A1340F16FCA) and an isolator are placed after the two-stage amplifier to ensure the out-of-band rejection of the channel. The temperature compensation attenuator is used to adjust the gain variation under temperature changes. The mixer (MINI's MCA1-24MH+) is a double-balanced mixer. A low-pass filter (MINI's XLF-151+) is cascaded after mixing to avoid excessive leakage of the local oscillator at the IF port, which results in channel saturation. An amplifier (MINI's PGA-103+) is added to the IF, so that the total channel gain can meet the design requirements. The channel finally uses an LC band-pass filter to ensure the out-of-band rejection indicator.

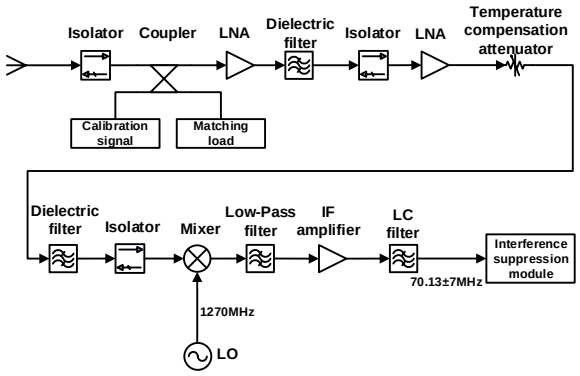

Fig. 17. The working principle of the receiving channel.

The NF of the receiving channel, the amplitude and phase consistency between the receiving channels and the isolation of the channels have great influences on the interference suppression performance. In the current design, the NF of the receiving channel is better than 1.5dB; the amplitude consistency between receiving channels is better than 0.5dB; the phase consistency is better than 5°. By using the metal sub-cavity design for each receiving channel, the isolation between channels is better than 70dB.

The transmitting up-conversion module includes a transmitting channel which converts the 70.13 MHz IF calibration signal output by the baseband module to the 1341.13MHz RF signal and adjusts the output signal to a suitable power level range. After power dividing and coupling, they act as the calibration signal for the seven receiving channels. The working principle of the transmitting channel is shown in Fig. 18. The local oscillator signal frequency is 1270MHz. The device has a high isolation between local oscillator and RF. The IF signal power is not high, which can guarantee the linearity. The filters are designed before and after the mixer to ensure the purity of the signal after mixing. The RF amplifier is Qorvo's TQP3M9036 and the local oscillator driver amplifier is NC3046S.

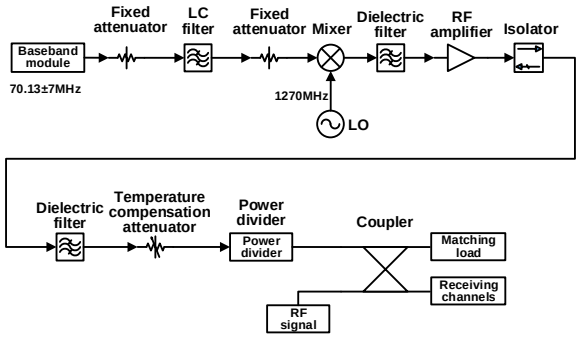

Fig. 18. The working principle of the transmitting channel.

The local oscillator module consists of a phase-locked crystal oscillator (Haichuang's PDS100MHz) and a phase-locked point source. The working principle of the local oscillator module is shown in Fig. 19. To generate 100MHz reference signals for both the phase-locked point source and baseband module, the 10MHz reference signal is phase-locked by using a thermostatic phase-locked crystal, ensuring low phase noise. After the 100MHz reference signal being amplified and filtered, it is used as the clock signal of the baseband and interference suppression module of the latter stage. The phase-locked point source locks the 100MHz reference signal generates a 1270MHz RF signal. After power dividing and amplification, they are used as the local oscillator signal of the mixers for the receiving and transmitting channels. The function of the attenuator is to control the power of the local oscillator signal and prevent the local oscillator signal input end of the mixer from being overloaded.

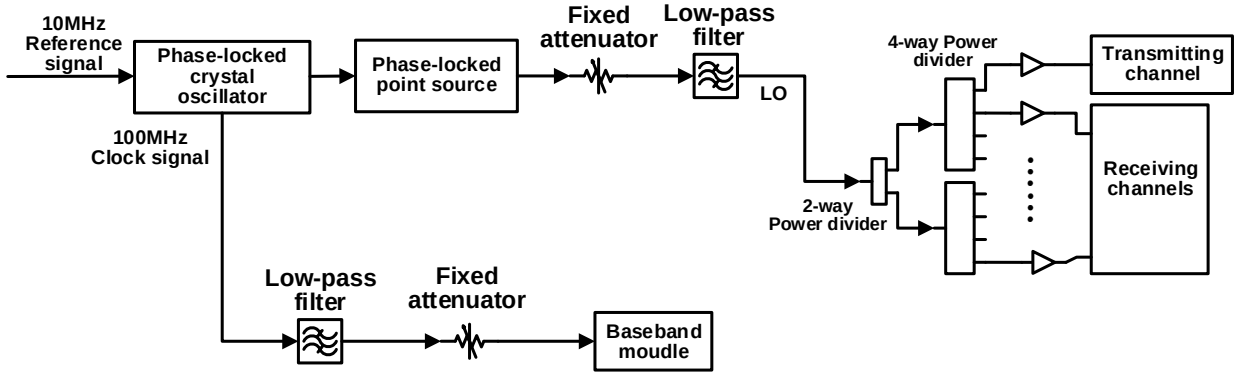

Fig. 19. The working principle of the local oscillator module.

C. Interference suppression module

The interference suppression module has two working modes of channel correction and interference suppression. Figure 20 depicts the block diagram of the interference suppression module. And the prototype of the interference suppression module is shown in Fig. 21.

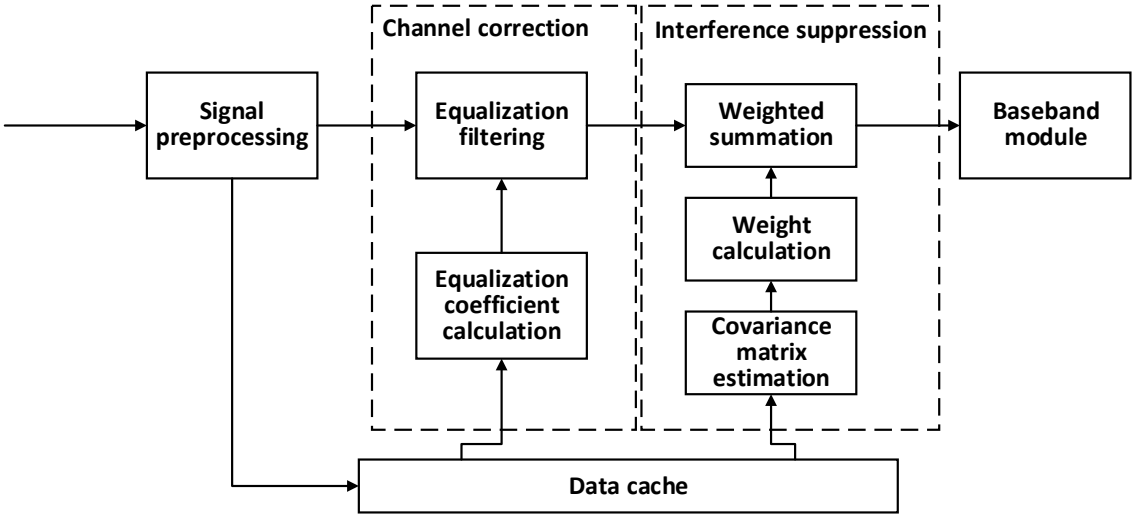

Fig. 20. The block diagram of the interference suppression module.

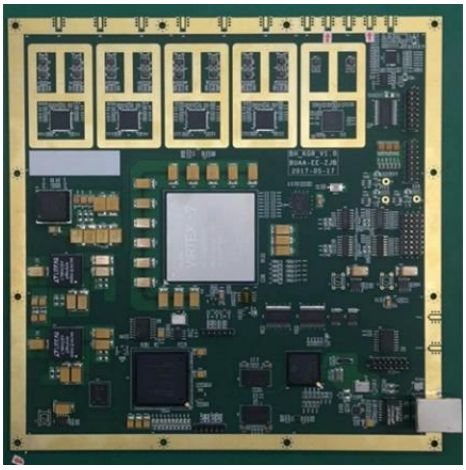

Fig. 21. The prototype of the interference suppression module.

The interference suppression module hardware board includes seven high-speed AD input channels, one high-speed DA output channel, FPGA logic unit, DSP control unit, clock management unit and power management unit. The bit-width of AD determines whether the sampling of the signal is complete or not. And the data processing resources of FPGA and DSP determine whether the interference suppression operation can be performed on the sampled data or not. The device selected in this paper can meet the requirements of interference suppression. The maximum sampling rate, bit-width, and channel isolation of the AD (ADS42LB69) input channel are 250MSPS, 16Bit, and 80dB, respectively. The maximum sampling rate, bit-width, and channel isolation of the DA (AD9142A) output channel are 1600MSPS, 16Bit, and 80dB, respectively. The FPGA is Xilinx's XC7V690T, and the DSP is TI's TMS320C6747.

In the channel correction mode, the baseband module generates the IF calibration signal. The signal is up-converted to the RF through the transmitting channel. Then the power is divided to seven channels, and coupled to each of the receiving channels. Based on the time domain channel equalization algorithm, the coefficients of the equalization filters of each channel are calculated. These coefficients are written into the FPGA by the DSP to complete the channel correction.

In the interference suppression mode, the LCMV-PI algorithm is used to perform anti-jamming processing on the received signal. The processed data is transmitted to the back-end baseband module for acquisition and tracking.

IV. IMPLEMENTATION AND RESULTS

In order to verify the performance of the algorithm and the design accuracy of the anti-jamming front-end, the performance of channel equalization and interference suppression of the proposed device are tested after the design and production. The prototype and the test environment of the proposed anti-jamming front-end are illustrated in Fig. 22 and Fig. 23 respectively.

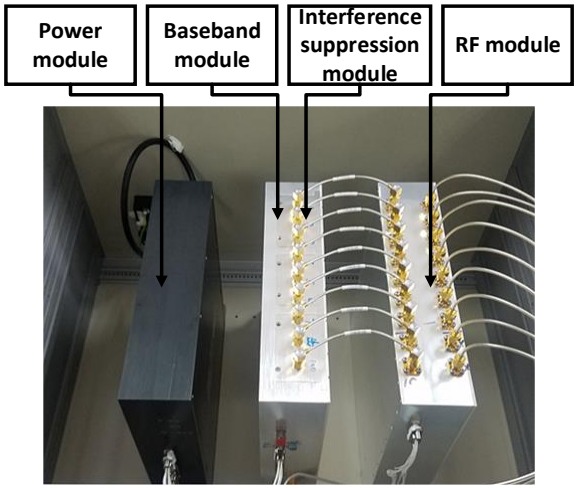

Fig. 22. The prototype of the proposed anti-jamming front-end.

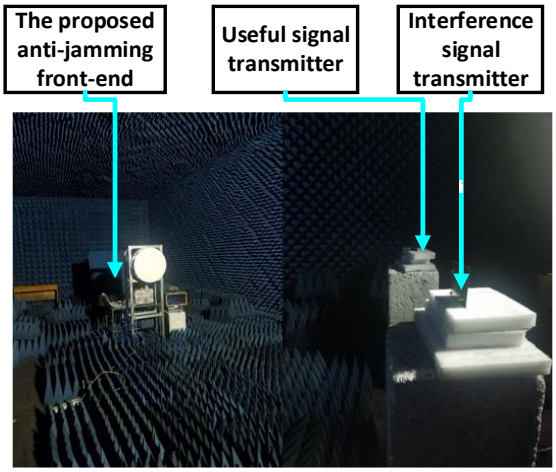

Fig. 23. The test environment of the proposed anti-jamming front-end.

A. The performance of channel equalization

The test method is as follows. Firstly, the same equalized signal are input to seven RF receiving channels. Then, the cancellation ratio (CR) of the output signals with and without the equalizing filter are compared. The test results are shown in Table 1. It can be seen that, the channel equalization has an improvement of more than 20 dB on the channel inconsistency, which will help improve the anti-jamming performance.

Table 1: The test results of the CR

Receiving Channel	2	3	4	5	6	7
CR before equalization (dB)	-13.4275	-8.9577	-22.9154	-16.7140	-7.3931	-15.5315
CR after equalization (dB)	-37.4985	-34.2868	-40.7181	-40.1475	-33.6433	-38.8989

B. The performance of interference suppression

We first start the useful signal transmitter, gradually reduce the signal power, and test the threshold of the receiver system. Then, the signal is fixed to the threshold power, and the interference signal transmitter is turned on. The interference signal power is gradually increased, and the interference suppression capability of the receiver system is tested. Through testing, we obtained that when the angle between the useful signal and the interference signal is 8°, 12°, and 16°, the interference suppression capability of the device reaches 69dB, 74dB, and 80.5dB, respectively. Table 2 lists the performance comparison among the anti-jamming front-end, including the algorithm, the angle between directions of the useful signal and interference signal and the interference suppression capability. Results indicate that the present work has better interference suppression capability at the smaller angle.

Table 2: Performance comparison of the anti-jamming front-end

Item	[18]	[19]	[20]	Our Work
Algorithm	Sub-band adaptive filter	LMS	SWGQR-RLS	LCMV-PI
ΔΦ	90°	10°	30°	8°
Interference suppression capability	ISR=84dB	ISR=60dB	ISR=40dB	ISR=69dB

It can be seen that the proposed anti-jamming front-end can effectively suppress the interference, and then improve the performance of the satellite navigation receiver.

V. CONCLUSION

In this paper, we proposed an anti-jamming front-end prototype for satellite navigation receiver. The interference suppression technique based on the LCMV-PI algorithm is applied to the interference suppression module. Considering that the channel inconsistency may have a bad influence on the interference suppression effect and the back-end signal acquisition and tracking, the channel correction function based on the channel equalization algorithm is designed. The test results show that the designed anti-jamming front-end can effectively suppress the interference signal and improve the anti-jamming performance of the satellite navigation receiver.

REFERENCES

[1] M. Cuntz, A. Konovaltsev, and M. Meurer, "Concepts, development, and validation of multi-antenna GNSS receivers for resilient navigation," *Proceedings of the IEEE*, vol. 104, no. 6, pp. 1288-1301, June 2016.

[2] I. J. Gupta, I. M. Weiss, and A. W. Morrison, "Desired features of adaptive antenna arrays for GNSS receivers," *Proceedings of the IEEE*, vol. 104, no. 6, pp. 1195-1206, June 2016.

[3] C. Fernández-Prades, J. Arribas, and P. Closas, "Robust GNSS receivers by array signal processing: Theory and implementation," *Proceedings of the IEEE*, vol. 104, no. 6, pp. 1207-1220, June 2016.

[4] L. M. Li and L. B. Milstein, "Rejection of narrow-band interference in PN spread-spectrum systems using transversal filters," *IEEE Transactions on Communications*, vol. 30, no. 5, pp. 925-928, May 1982.

[5] L. B. Milstein, "Interference rejection techniques in spread spectrum communications," *Proceedings of the IEEE*, vol. 76, no. 6, pp. 657-671, June 1988.

[6] D. B. Rao and Sun-Yuan Kung, "Adaptive notch filtering for the retrieval of sinusoids in noise," *IEEE Transactions on Acoustics, Speech, and Signal Processing*, vol. 32, no. 4, pp. 791-802, Aug. 1984.

[7] H. V. Poor, "Active interference suppression in CDMA overlay systems," *IEEE Journal on Selected Areas in Communications*, vol. 19, no. 1, pp. 4-20, Jan 2001.

[8] Q. Chang, H. Wang, and X. X. Li, "The review of interference suppression algorithms about navigation receiver navigation," *Position and Timing*, vol. 4, no. 05, pp. 83-88, 2017.

[9] R. L. Fante and J. J. Vaccaro, "Wideband cancellation of interference in a GPS receive array," *IEEE Transactions on Aerospace and Electronic Systems*, vol. 36, no. 2, pp. 549-564, Apr. 2000.

[10] J. S. Goldstein, I. S. Reed, and L. L. Scharf, "A multistage representation of the Wiener filter based on orthogonal projections," *IEEE Transactions on Information Theory*, vol. 44, no. 7, pp. 2943-2959, Nov. 1998.

[11] W. L. Shi, Y. S. Li, and J. W. Yin, "Improved constraint NLMS algorithm for sparse adaptive array beamforming control applications," *Applied Computational Electromagnetics Society Journal*,

34.3, 2019.

[12] W. Choi, T. K. Sarkar, Hong Wang, and E. L. Mokole, "Adaptive processing using real weights based on a direct data domain least squares approach," *IEEE Transactions on Antennas and Propagation*, vol. 54, no. 1, pp. 182-191, Jan. 2006.

[13] Y. Xiao-bo, "An improved GPS receiver anti-jammer algorithm based on space-time adaptive processing," *2012 International Conference on Computer Distributed Control and Intelligent Environmental Monitoring*, Hunan, pp. 106-109, 2012.

[14] S. Leng and Wee Ser, "Adaptive null steering beamformer implementation for flexible broad null control," *Signal Processing*, 91.5, pp. 1229-1239, 2011.

[15] L. Zhao, Y. Mao, and J. Ding, "A STAP interference suppression technology based on subspace projection for BeiDou signal," *2016 IEEE International Conference on Information and Automation (ICIA)*, Ningbo, pp. 534-538, 2016.

[16] S. Daneshmand, A. Jahromi, A. Broumandan, and G. Lachapelle, "GNSS space-time interference mitigation and attitude determination in the presence of interference signals," *Sensors*, 15.6, pp. 12180-12204, 2015.

[17] H. Wang, L. Yang, Y. Yang, and H. Zhang, "Anti-jamming of Beidou navigation based on polarization sensitive array," *2017 International Applied Computational Electromagnetics Society Symposium (ACES)*, Suzhou, pp. 1-2, 2017.

[18] Y. T. Liu, "Satellite navigation antenna and adaptive anti-jamming technology," *Beijing University of Posts and Telecommunications*, 2019.

[19] J. H. Xiang, "Research on application of GPS nulling technology based on space-time adaptive processing," *Harbin Engineering University*, 2009.

[20] B. B. Shi, "Research on the technologies of high degrees of freedom interference suppression for GNSS receiver," *National University of Defense Technology*, 2011.